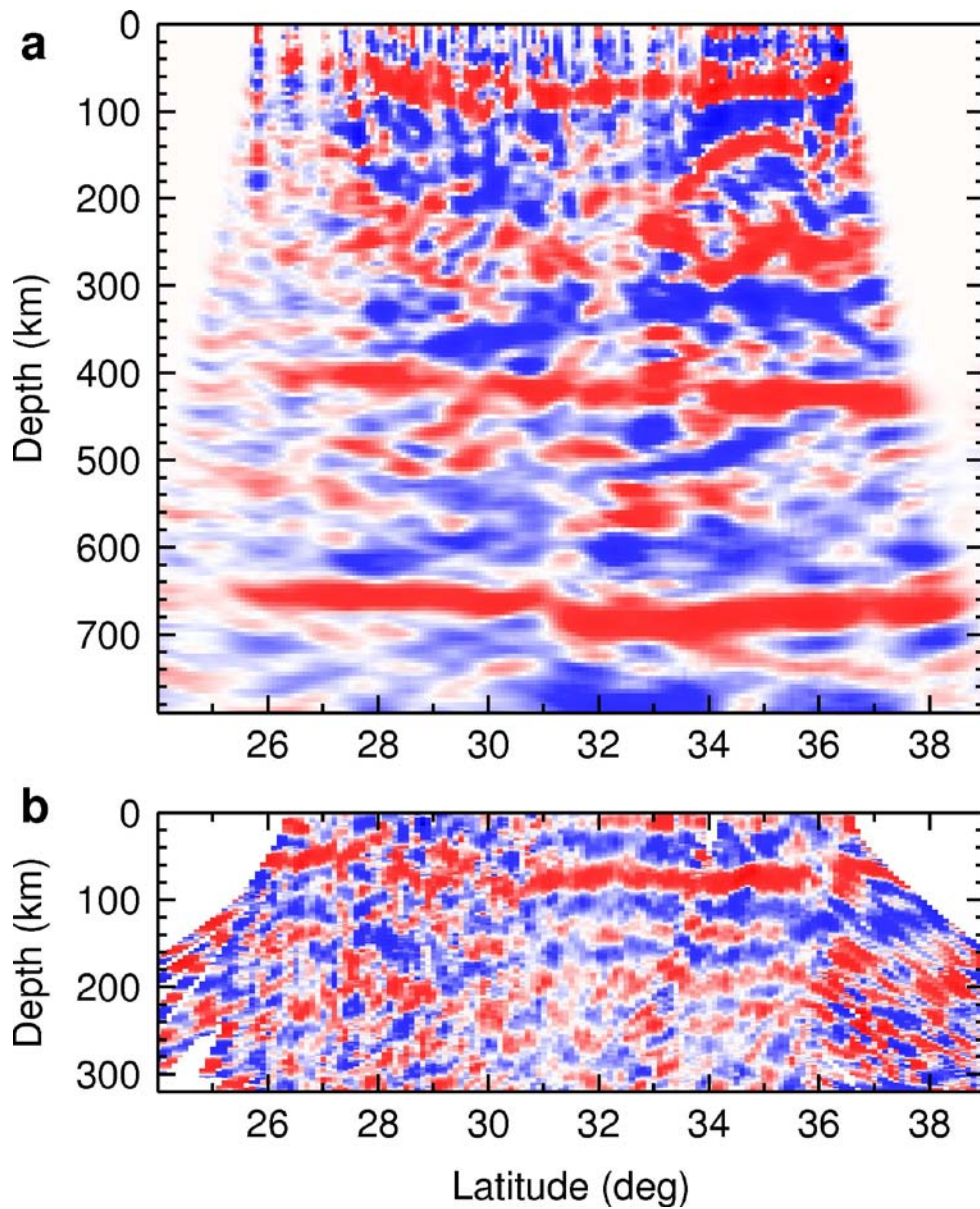# Tibetan plate overriding the Asian plate in central and northern Tibet

Wenjin Zhao, Prakash Kumar, James Mechie, Rainer Kind, Rolf Meissner, Zhenhan Wu, Danian Shi, Heping Su, Guangqi Xue, Marianne Karplus, Frederik Tilmann

Corresponding Author: R. Kind, email:kind@gfz-potsdam.de

Figure S1. Data shown in Fig.2 of the main text without any correlations marked. All available data along the INDEPTH line are used. a) P receiver functions, b) S receiver functions.
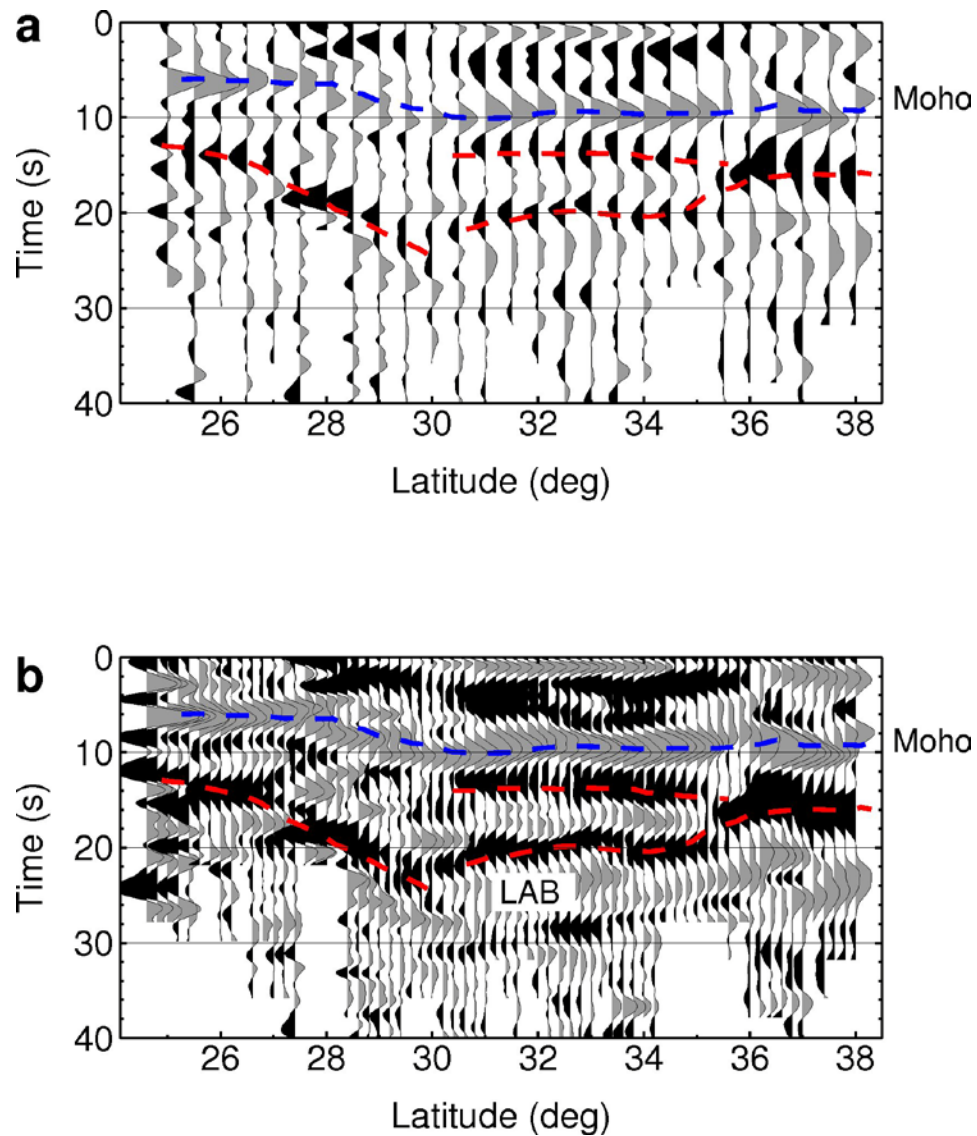
Figure S2. Summed S receiver functions along the INDEPTH line in the time domain. The size of the summation window is 1 degree. Blue dashed line - Moho; red dashed lines - LAB of the different plates. a) windows moved by 0.5 degrees, b) windows moved by 0.2 degrees.

3
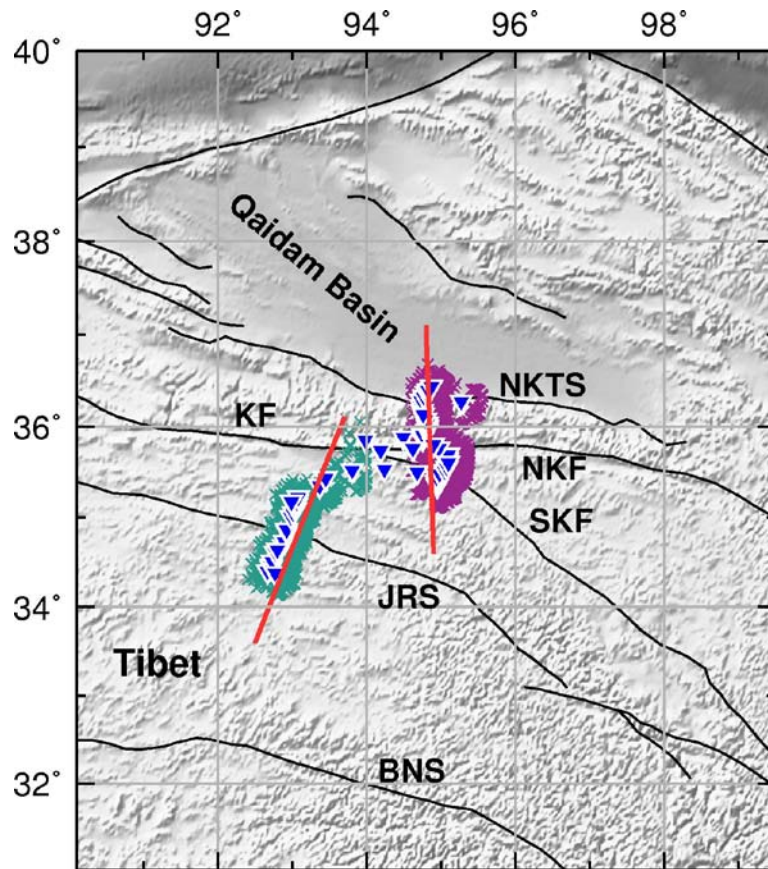
Figure S3. Location of the INDEPTH IV stations (triangles) and locations of Moho piercing points of P receiver functions at 70 km depth. Key: BNS – Banggong-Nujiang Suture, JRS – Jinsha River Suture, SKF – South Kunlun Fault, NKF – North Kunlun Fault, KF – Kunlun Fault, NKTS – North Kunlun Thrust System.
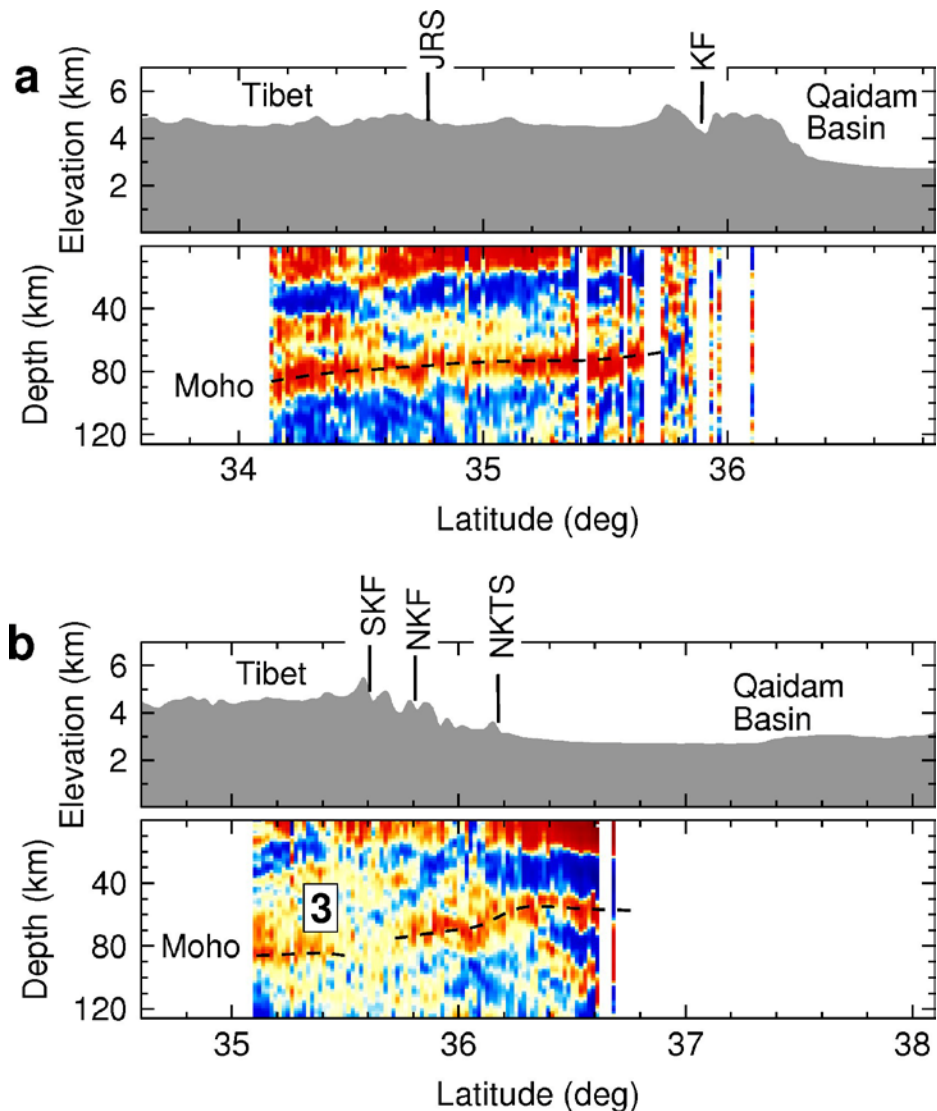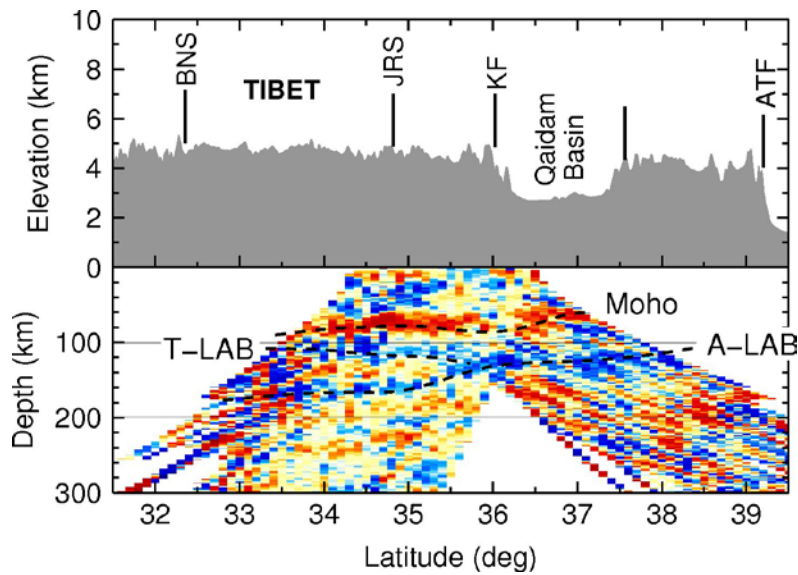
Figure S4. INDEPTH IV P-receiver functions in the time domain (depth obtained from the local model) along the two profiles marked in Figure S2. a) Profile across the Jinsha River Suture; b) Profile across the Kunlun Fault. The blue (negative) structure marked with number '3' (also marked in Fig. 2c in the main text) penetrates the entire crust from the surface to the Moho. It reaches the surface at the North Kunlun Thrust System (NKTS). This structure is inclined to the south. It probably indicates the existence of lower velocity upper crustal material from the Qaidam basin below higher velocity material from northern Tibet. The Moho and LAB rise towards the Qaidam basin below this structure. Key: see Fig. S3.
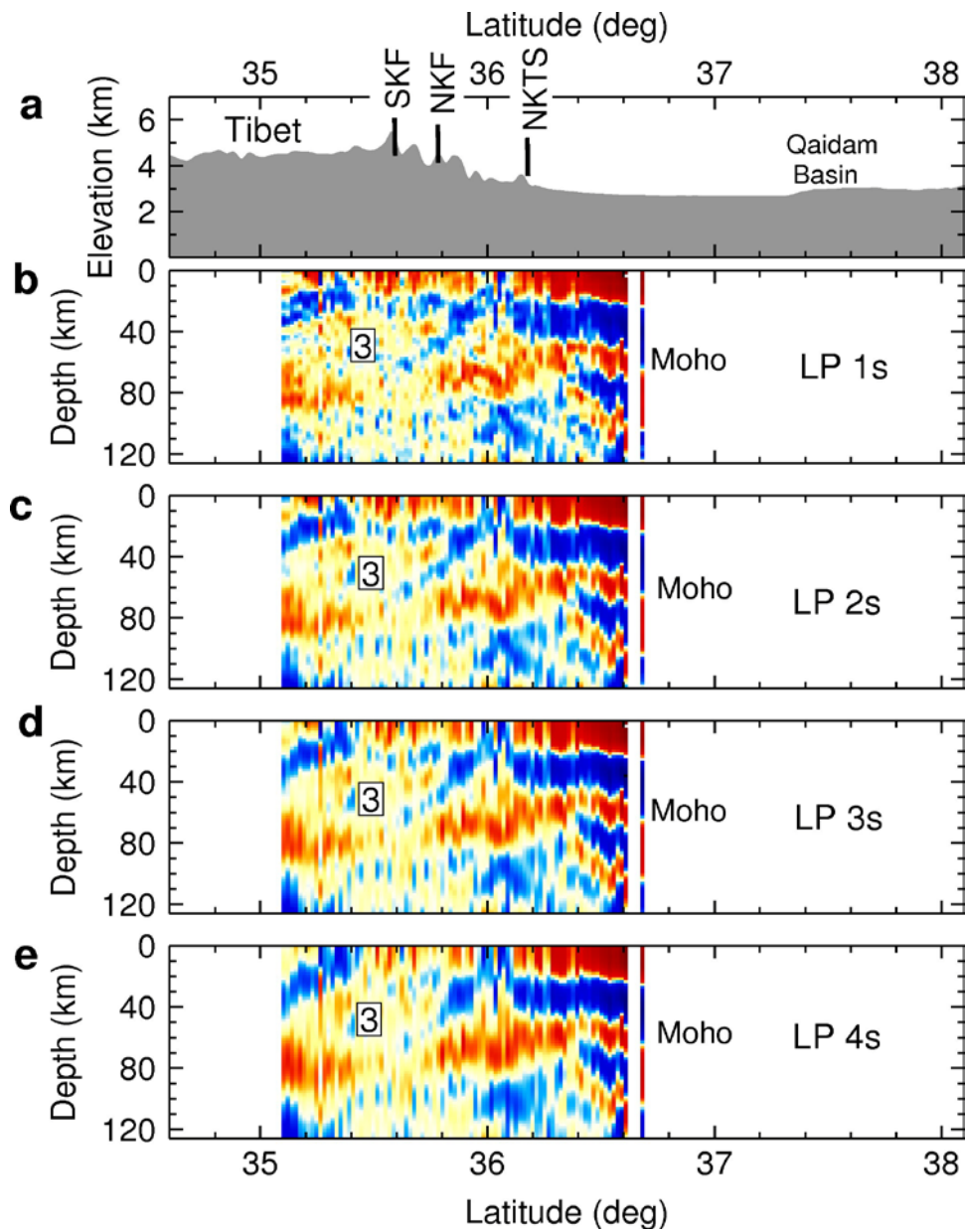
Figure S5. Same as in Fig.2c but for several filters. The blue discontinuity marked with number '3' remains stable. The Moho is weak where it is reached by the inclined structure. Key: see Fig. S3.
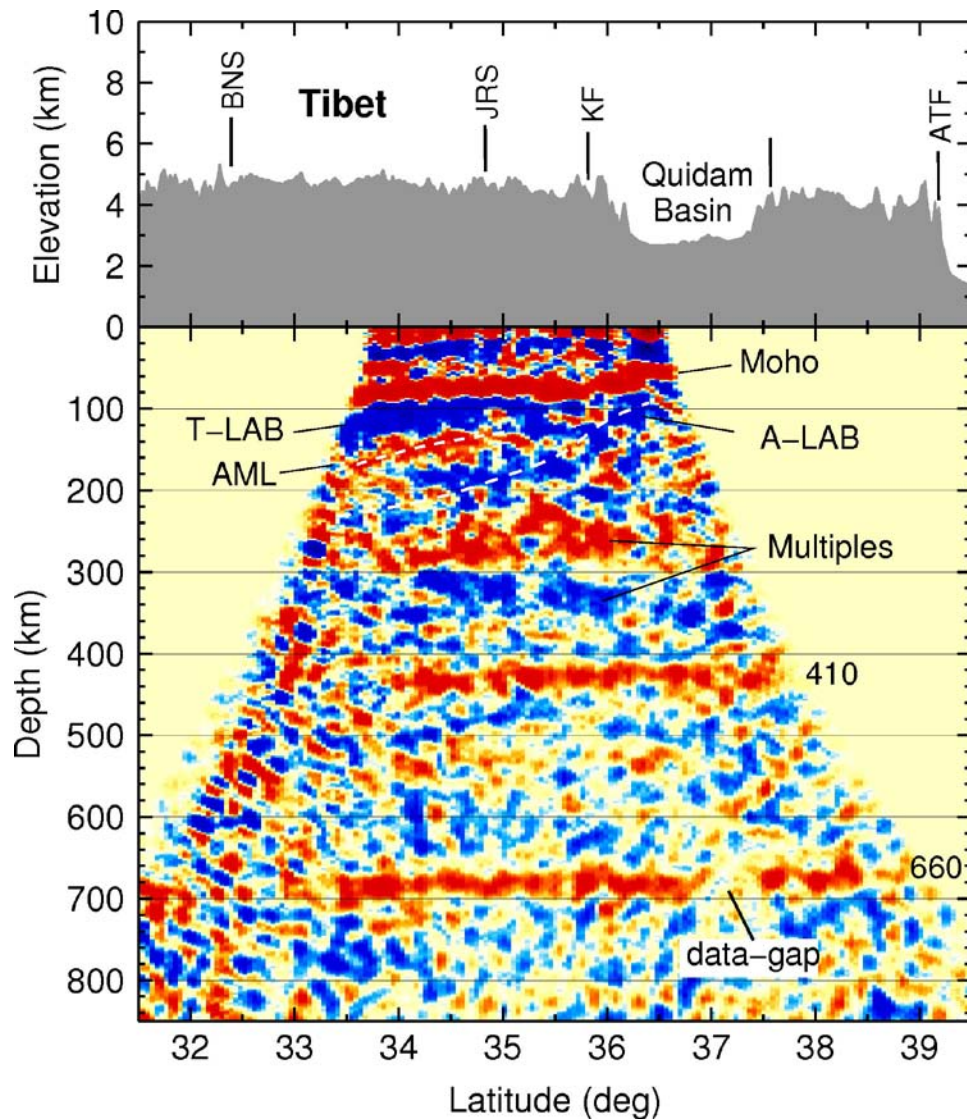
Figure S6. Migrated P receiver functions down to 800 km depth. Only INDEPTH IV data are used. Key: see Fig. S3 and T-LAB = Tibetan LAB, A-LAB = Asian LAB, AML = Moho of subducting Asian plate, ATF – Altyn Tagh Fault.

7

Figure S7. Migrated S receiver functions along the two profiles in Figure S3. Only INDEPTH IV data are used. An abrupt deepening of the Moho towards the south is clearly visible, as is the splitting of the Asian LAB towards the south into two low velocity structures (the deepening Asian LAB and the shallower Tibetan LAB). Key: see Figs. S3 and S6. The main features (Moho, A-LAB and T-LAB) are well resolved in P and S receiver function images (Figs.S6 and S7).

8
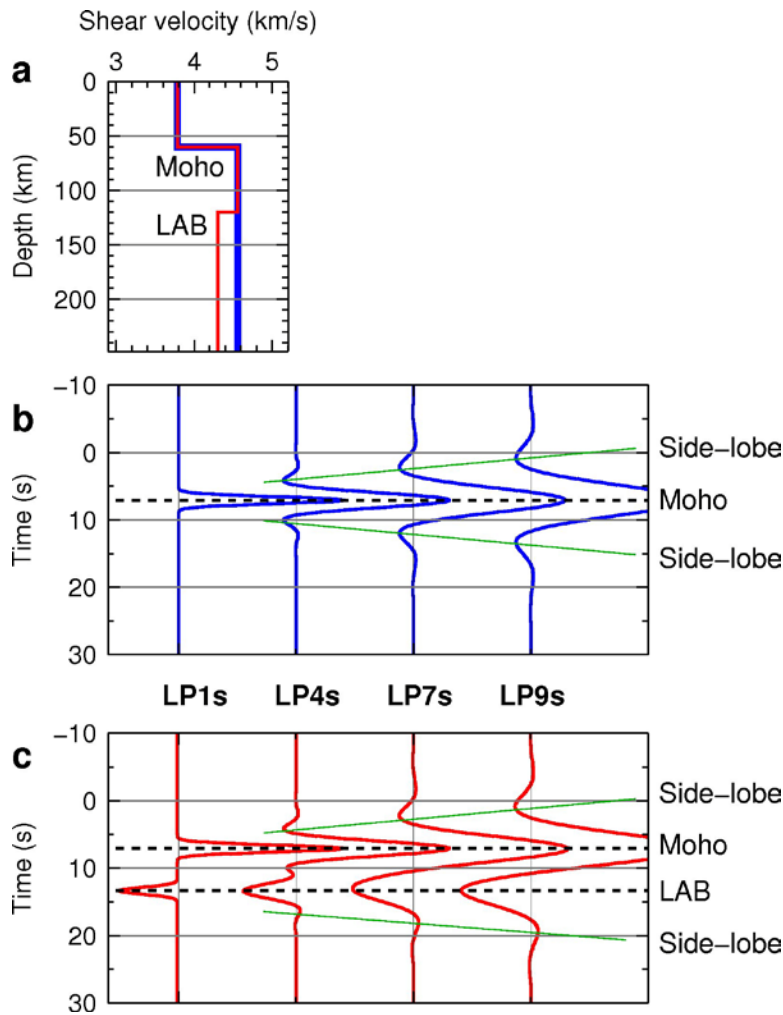
**Figure S8.** Synthetic test to show effects of side lobes due to filtering. The synthetic S-receiver functions have been generated for the two models shown in a) with Moho+half-space (blue) and with Moho+lid+half-space (red). We applied a suite of Butterworth filters of order 3 to the synthetics in the same way as we have treated the real data. The traces corresponding to the filters are marked as LP1s (implies low-pass filter with period 1sec), LP4s, LP7s and LP9s. In b) we have only one discontinuity and towards longer periods we have larger side-lobes (marked by green lines) with increasing time separation from the main phase. In c) the LAB overwhelms the side lobe and the moveout of the side lobe with increasing periods becomes essentially insignificant.

9
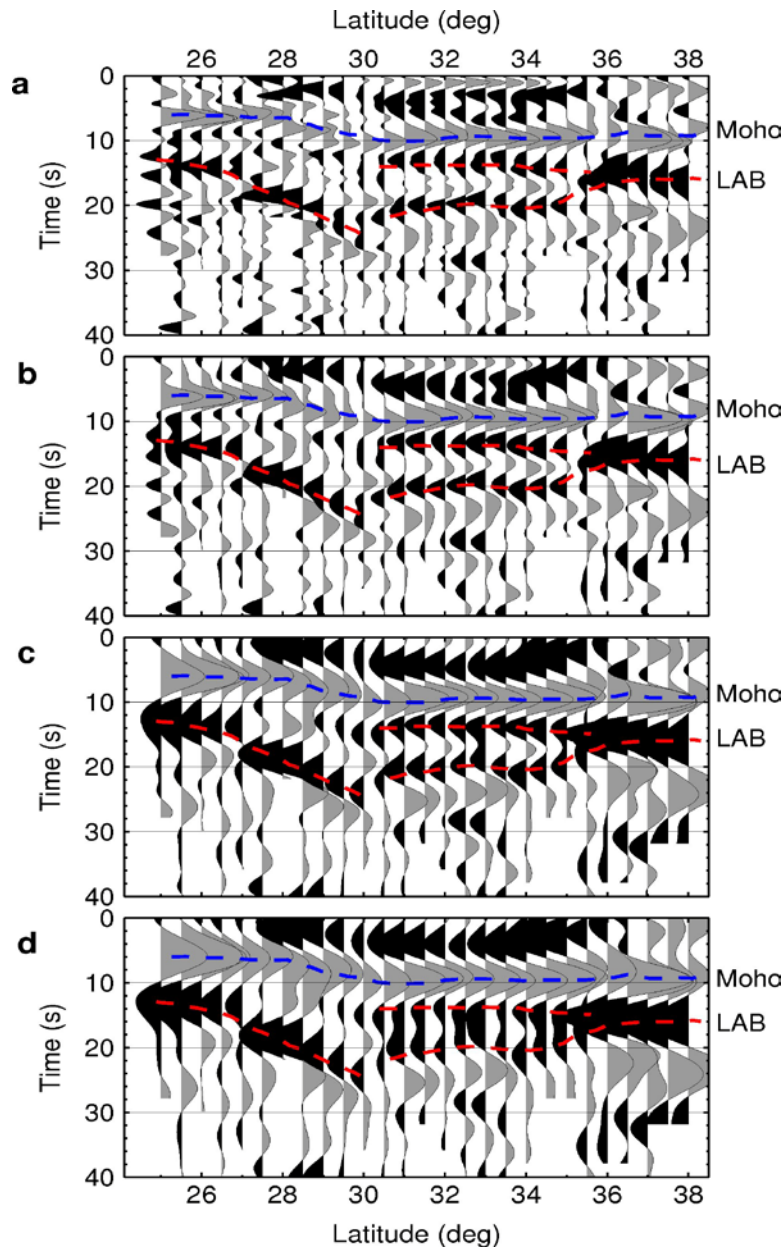
Figure S9. Same as Figure S2a but here we plotted with four different low-pass filters with corner periods of a) 1sec, b) 4sec, c) 7sec and d) 9sec. The dashed lines (interpreted discontinuities in blue and red) always follow the main identified phases independent of the period and thus confirm that the said phases are not side-lobes from the Moho. The typical increasing moveout of side lobes with increasing wavelength is not visible.

10
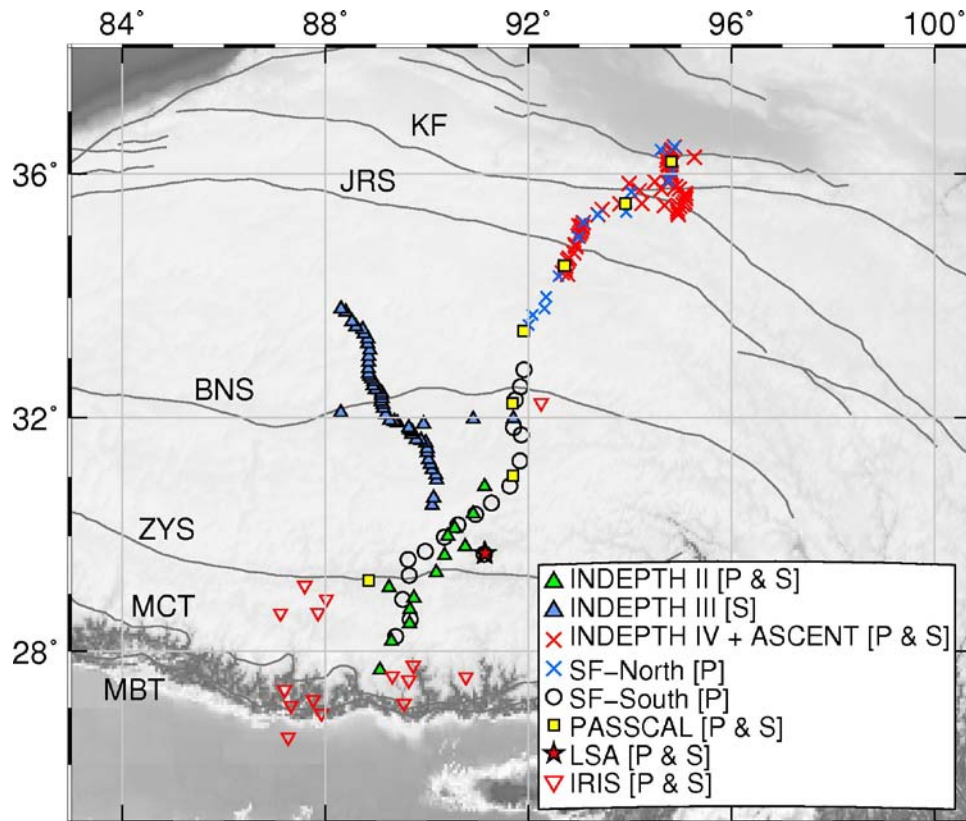
Figure S10. Distribution of stations from the different projects which contributed data to the present work; P=P receiver functions, S=S receiver functions:
INDEPTH II: Kind et al. (1996)
INDEPTH III: Kind et al. (2002),
INDEPTH IV+ASCENT: Zhao et al. (2008).
SF-North: Wittlinger et al. (1996), Kind et al. (2002)
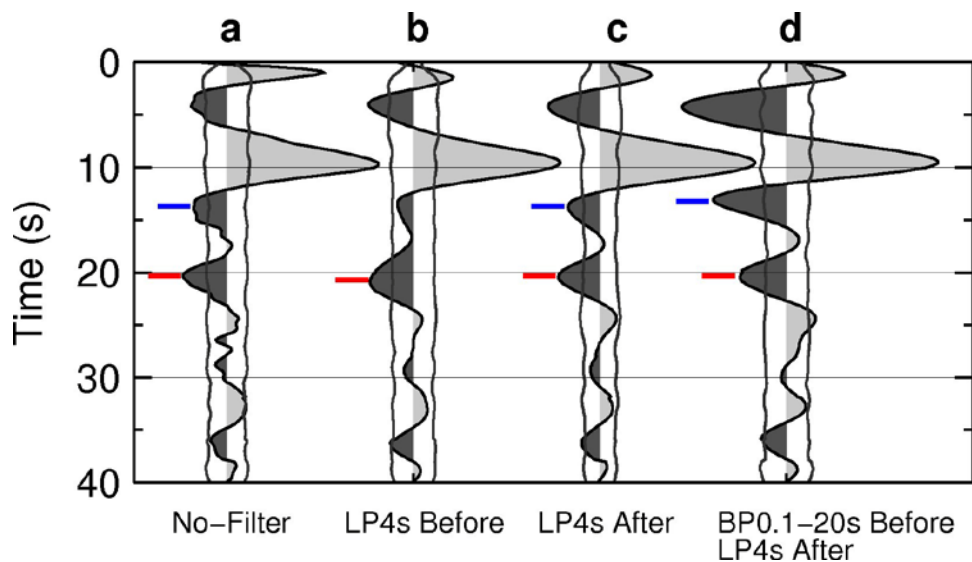SF-South: Hirn et al. (1995), Kind et al. (2002)
PASSCAL: Owens et al. (1993)
LSA: Station Lhasa of IRIS/USGS/CDSN Seismic Network
IRIS: Stations from the following networks:
Himalayan Nepal Tibet Experiment
China National Seismic Network
Bhutan Temporary Network

11

Figure S11. Influence of filtering on receiver function data before and after deconvolution. Data from Fig.S1 between 29°N and 32°N have been stacked. a) raw broadband data are used, b) low pass filter with corner period at 4s (LP4s) is applied before deconvolution. c) LP4s filter is applied after deconvolution. The two negative signals marked by red and blue dashes differ considerably. The signal marked blue has almost disappeared in trace b. This means the result of processing may not be independent of the sequence of processing steps, probably due to the approximate nature of the deconvolution. Filtering after deconvolution (trace c) is very similar to trace a) with no filter, which is therefore preferable. Trace d) shows data filtered with a bandpass between 0.1s and 20s before deconvolution and LP4s filter after deconvolution to smooth the trace. These filtering steps have been used in the present work. Kumar et al. (2006) used filtering steps like in b). Therefore the blue negative signal is only barely visible in their data. The two parallel lines running on both side of the traces are the ±2Standard errors.

12

References

A. Hirn et al., Nature 375, 571 (1995).

R. Kind et al., Science 274, 1692 (1996).

R. Kind et al., Science 298, 1219-1221 (2002).

Kumar, P., Yuan, X., Kind, R. & Ni, J., J. Geophys. Res. **111**, B06308 (2006).

T. J. Owens, G. E. Randall, F. T. Wu, R. Zeng, Bull. Seismol. Soc. Am. 83, 1959 (1993).

G. Wittlinger et al., Earth Planet. Sci. Lett. 139, 263 (1996).

W. Zhao et al., EOS Trans. Am. Geophys. Union 48, 487-488 (2008).